AALBORG UNIVERSITY
STUDENT REPORT

NTNU

9th Semester

School of Information and Communication Technologies

Electronics and IT

Fredrik Bajers Vej 7C

9220 Aalborg

http://www.sict.aau.dk/electronics-and-it

Title:
Trajectory Planning for Cart Pendulum System

Theme:
Control Engineering

Project Period:
Autumn 2017
21/08/2017 - 21/12/2017

Participants:
Niels Skov Vestergaard

Supervisor:
Anton Shiriaev
John-Josef Leth

Pages:

Concluded: 21/12/2017

Synopsis

The aim of the project was to investigate a method for trajectory planning for a cart pendulum. To find an interesting trajectory, a task was posed for the system to complete.
The system was modeled and a simulation of the system dynamics created using MATLAB Simulink. To aid in the progress and to be able to show the result in a visual manner a graphical layer was added to the simulation.
The properties of the system was assessed using phase portraits. It was found that the phase portrait can be altered making different trajectories possible by designing the input force as a solution to the integral of the system dynamics given some initial conditions and constraints.

Contents

1 | Introduction

2 | The System

In this chapter, the system is presented, along with a brief overview of the hardware provided in the setup.

2.1 System Setup

A system is provided by the automation and control department at Aalborg University (AAU). The setup is seen in Figure 2.1, the parameters that can be measured directly are indicated.

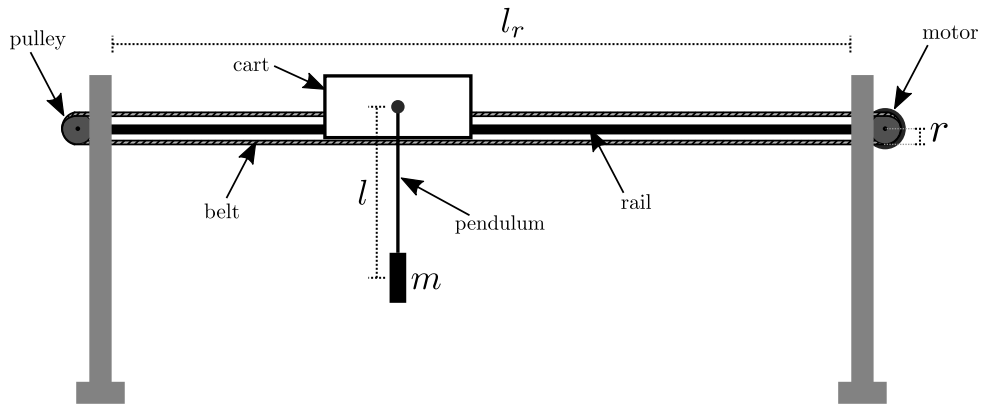

Figure 2.1: The system setup provided by AAU, where m is the mass of the pendulum weight attached at the end of the rod, l is the length from pivot point to center of mass, r is the radius of the pulley and l_r is the effective length of the rail.

The mass of the cart cannot be directly measured as it is preferred not to take the system apart. This parameter is later estimated along with frictions in the system. [1]

[2]

2.2 Motors

There are two Maxon 370356 brushed DC motors, see Figure 2.2, used in the setup. [3].

[4]

[1] FiXme Note: streamline friction notation, see sources
[2] FiXme Note: add picture of the system (showing wires on cart)
[3] FiXme Note: source
[4] FiXme Note: see url source in comment

Figure 2.2: maxonMotor

The most interesting characteristic of the maxon motor for the purposes of this report are shown in Table 2.1.

Characteristic	**Quantity**	**Unit**
Nominal torque (max. continuous torque)	420×10^{-3}	$\mathrm{N} \cdot \mathrm{m}$
Nominal current (max. continuous current)	4.58	A
Torque constant	93.4×10^{-3}	$\mathrm{N} \cdot \mathrm{m} \cdot \mathrm{A}^{-1}$
Rotor inertia	54.2×10^{-6}	$\mathrm{kg} \cdot \mathrm{m}^2$
Weight	1.1	kg

Table 2.1: '*' indicates that the parameter is estimated.

One of the motors is mounted on a pulley driving the belt, see Figure 2.1. The other motor is disabled and acts only as a bearing at the pendulum pivot point.

2.3 Motor Encoders

Each of the two motors are equipped with an HEDS 5540 optical quadrature encoder, see Figure 2.2. The moment of inertia added by the encoder is negligibly small at only $0.6 \times 10^{-6}\,\mathrm{kg} \cdot \mathrm{m}^2$ and is not mentioned further in this report.

[5]

Figure 2.3: encoder

[5] FiXme Note: see url source in comment

2.4 Motor Controller

Two Maxon ADS 50/10 motor controllers, see Figure 2.4, are mounted on the cart pendulum setup. One on the side to control the driving motor and the other, not used in this project, mounted on the cart. The datasheet states that the motor controller weights 0.38 kg, but again, since the remaining mass of the cart is unknown and can not be measured, the cart mass must be estimated.[6]

[7]

Figure 2.4: maxonMotorController

The motor controller can be configured in four different modes,

- Speed control using tacho signals
- Speed control using encoder signals
- IxR compensated speed control
- Torque or current control

The first three modes are forms of speed control while the last is current control relating directly to torque and thereby also force on the belt. The chosen mode for this project is therefore current control. The conversion from armature current to motor torque is by use of the torque constant given in Table 2.1. To set the armature current the motor controller requires a ± 10 V input signal. This input is provided through a shield from the microcontroller, so the conversion to armature current is handled in the following.[8]

2.5 Micro Controller

The control design is implemented on a Teensy 3.6 microcontroller, see Figure 2.5, provided in the setup. The armature current reference is provided through one of the microcontroller's two 12 bit DAC's (Digitl-to-Analog Converter) placed on an external pin of the microcontroller. The Teensy 3.6 runs on 3.3 V provided by an onboard regulator

[6] FiXme Note: source
[7] FiXme Note: see url source in comment
[8] FiXme Note: source

from 5 V USB supply, and so the analog output is in the range of 0−3.3 V with a 12 bit resolution.
The motor encoders are decoded on the shield, see next section, and read through an 8 bit parallel data bus by the microcontroller.

[9]

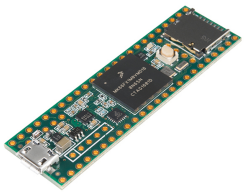

Figure 2.5: teensy3.6

The Teensy 3.6 uses a bootloader which allows programming through USB using the Teensyduino add-on for the Arduino IDE.

2.6 Shield

A shield located by the microcontroller handles conversion/interfacing between the microcontroller and the setup. The motor encoders are decoded using Avago HCTL-2021-PLC decoders, mounted on the shield, which outputs 2000 ticks pr. revolution.[10] This results in a resolution of $2\pi/2000 = \pi \times 10^{-3}$ rad/tic, for the pendulum angle, θ, and $2\pi r/2000 = 2\pi \cdot 0.028/2000 \approx 0.088 \times 10^{-3}$ m/tic for the position along x. The armature current reference is provided from the microcontroller which as mentioned outputs 0−3.3 V while the motor controller requires a ±10 V input. This is handled by an amplification on the shield converting the 0−3.3 V to the required ±10 V. A previous project group has tested the relation between armature current and different 12 bit values from the micro controller. The test was conducted using a current clamp and an oscilloscope to measure the armature current in the motor. By linear regression they arrived at the following relation,

$$\text{bit}_{\text{DAC}} = 105.78 \cdot i_a + 1970 \quad . \tag{2.1}$$

An other way of measuring the current is from an output directly on the motor controller. It is found that this output is slightly different than the current measured directly over the motor using a current clamp. It is difficult to know if the torque constant supplied by the company is matched using one or the other way of measuring. So a test is conducted to verify Equation 2.1, in which the steady state hold force is measured directly on the cart using a luggage scale as an alternative Newton-meter. The results of the force test are seen in Figure 2.6 and 2.7 and a test journal is provided in [11].

[9] FiXme Note: source: https://www.sparkfun.com/products/14057
[10] FiXme Note: source
[11] FiXme Note: refference appendix

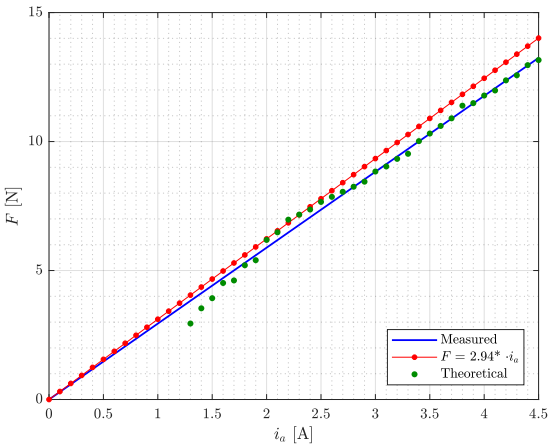

Figure 2.6: forceTest1

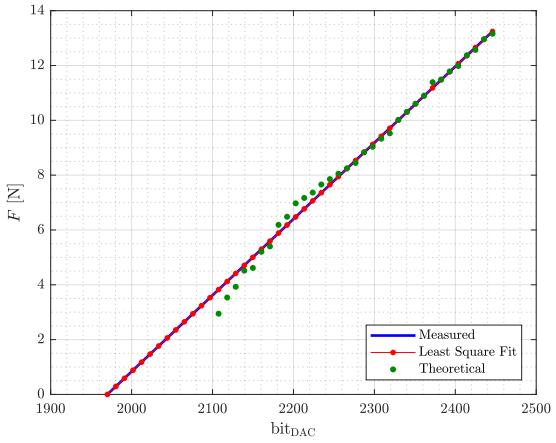

Figure 2.7: forceTest2

The measurements should be more correct at higher forces since friction then causes less disturbance in the measurements. However, no measurements are excluded in the regression as it is noted that the regression line fits the upper part of the data very well. Measurements lower than $F = 2.95$ were considered unreliable due to friction and therefore not included in the data-set. In Figure 2.6 the armature current is scaled using Equation 2.1 and the theoretical line is calculated using that $F = \frac{1}{r} k_\tau i_a$. As the theoretical line does not coincide exactly with the least square regression, Equation 2.1 is tweaked so that,

$$\text{bit}_{\text{DAC}} = 111.9 \cdot i_a + 1970 \quad , \tag{2.2}$$

which leads to the result seen in Figure 2.7, where the theoretical line now coincide with the least square regression of the measurement data.

3 | Problem Description

The system is underactuated, and nonlinear.

The system is presented with a specific task, see Figure 3.1. This aids in understanding the convinience of the presented trajectory planning tools, as the task requires nonlinear operation, where linearization alone is not enough.

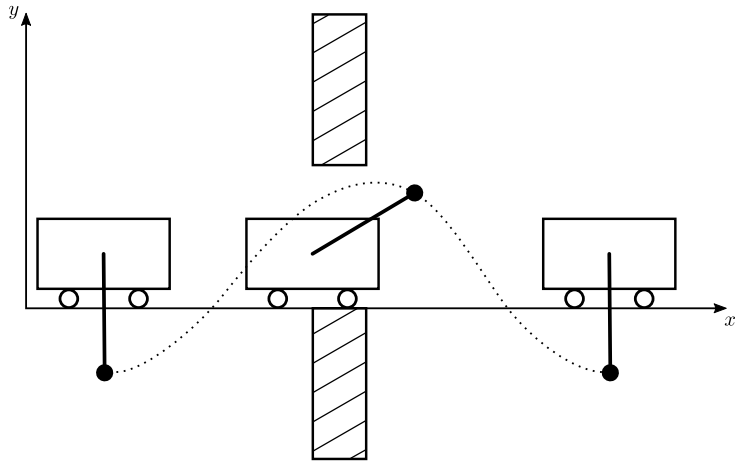

Figure 3.1: The task to be performed. The trajectory here is not realistic, and only shown to ilustrate the goal; avoiding the obstacles along the entire trajectory.

4 | Modelling

A dynamical model of the system is developed, first by Newton's method and then by the energy method. The model is simulated and the nonlinear nature of the system is investigated.
The model is based on the conventions presented in the mechanical diagram in Figure 4.2 while excessive coordinates are defined in Figure 4.1. The cart is constrained to the horizontal rail s.t. $y_c = 0$, that is, the cart only ever moves along the x-axis.

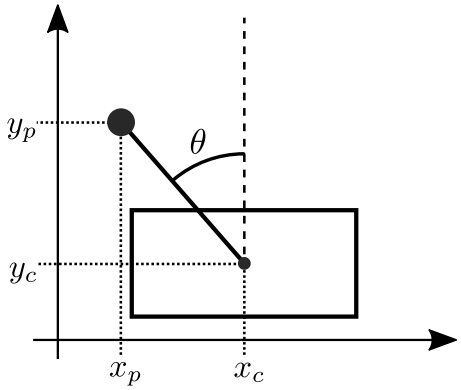

Figure 4.1: The cart pendulum system with excessive coordinates, where (x_c, y_c) is the position of pendulum pivot point on the cart and (x_p, y_p) is the position of the pendulum point mass.

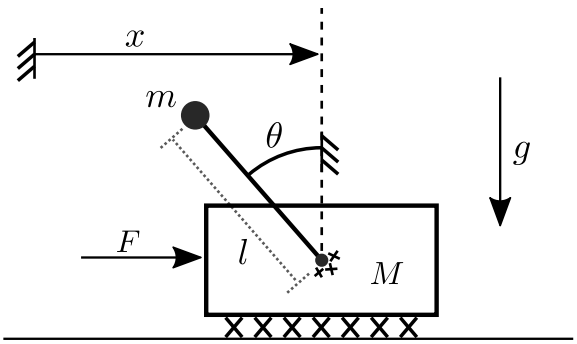

Figure 4.2: Mechanical drawing of the cart pendulum system with x and θ as generalized coordinates, where x is the center position of the cart, θ is the angle of the pendulum, m is the point mass of the pendulum, M is the mass of the cart, g is the gravitational acceleration and F is the force of actuation.

It is assumed that the pendulum rod is rigid and massless. This is deemed sensible, as the pendulum mass is much heavier than the hollow aluminum rod. The added inertia of the motor's rotor is also negligibly small, only $54.2 \times 10^{-6}\,\mathrm{kg \cdot m^2}$, see *Motors* section 2.2, compared to $ml = 0.201 \cdot 0.3348 = 67.3 \times 10^{-3}\,\mathrm{kg \cdot m^2}$ contributed by the pendulum mass. The pendulum mass is modeled as a point mass placed at its geometrical center. This is why the length, l, is measured from the pivot point to the center of the pendulum mass. The mass of the cart includes the weight of the belt and the wires hanging from the cart to the controller and supply. The influence of the wires will vary depending on the position of the cart, but this is treated as an unmodeled disturbance.
In the following two modeling approaches, fictions is represented as two unknown functions of generalized velocities, $\dot{x}$ and $\dot{\theta}$, denoted $B_c(\dot{x})$ for the cart and $B_p(\dot{\theta})$ for the pendulum. These functions are then modeled in section 4.3.

[1]

[1] FiXme Note: review if all assumptions are included

4.1 Newton's Method

Excessive coordinates - freebody diagrams in Figure 4.3 and 4.4

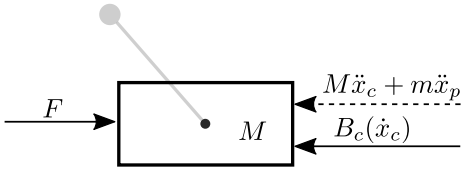

Figure 4.3: freeBodyCart

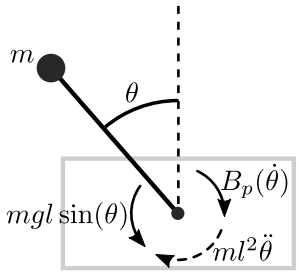

Figure 4.4: freeBodyPendulum

Newton's second law for the cart along x_c. Freebody diagram in Figure 4.3

$$M\ddot{x}_c + m\ddot{x}_p = F - B_c(\dot{x}_c) \tag{4.1}$$

Applying Newton's second law for rotational motion. Freebody diagram in Figure 4.4

$$ml^2\ddot{\theta} = mgl\sin\theta - B_p(\dot{\theta}) \tag{4.2}$$

Relation of D'alumbert forces for the pendulum decomposed as tangential forces,

$$-m\ddot{x}_p\cos\theta - m\ddot{y}_p\sin\theta = ml\ddot{\theta} \tag{4.3}$$

To combine Equation 4.3 and 4.2, Equation 4.3 is written as torques,

$$-ml\ddot{x}_p\cos\theta - ml\ddot{y}_p\sin\theta = ml^2\ddot{\theta} \tag{4.4}$$

Equation 4.3 and 4.2 are combined,

$$-ml\ddot{x}_p\cos\theta - ml\ddot{y}_p\sin\theta = mgl\sin\theta - B_p(\dot{\theta}) \tag{4.5}$$

The system dynamics is then represented using excessive coordinates by the following set of equations:

$$\begin{cases} -ml\ddot{x}_p\cos\theta - ml\ddot{y}_p\sin\theta = mgl\sin\theta - B_p(\dot{\theta}) \\ M\ddot{x}_c + m\ddot{x}_p = F - B_c(\dot{x}_c) \end{cases} \quad [\cdot] \tag{4.6}$$

Writing the excessive coordinates, Figure 4.1, in therms of the generalized coordinates, Figure 4.2,

$$\begin{cases} x_c &= x \\ y_c &= 0 \end{cases} \qquad \begin{cases} x_p = x - l\sin\theta \\ y_p = l\cos\theta \end{cases} \tag{4.7}$$

Finding the derivatives for the transformation,

$$\begin{cases} \dot{x}_p &= \dot{x} - l\cos\theta\dot{\theta} \\ \dot{y}_p &= -l\sin\theta\dot{\theta} \end{cases} \qquad \begin{cases} \ddot{x}_p = \ddot{x} + l\sin\theta\dot{\theta}^2 - l\cos\theta\ddot{\theta} \\ \ddot{y}_p = -l\cos\theta\dot{\theta}^2 - l\sin\theta\ddot{\theta} \end{cases} \tag{4.8}$$

Rewriting Equation 4.6 in generalized coordinates using the cooredinate transformation from Equation 4.7 and 4.8 yields,

$$\begin{cases} -ml(\ddot{x} + l\sin\theta\dot{\theta}^2 - l\cos\theta\ddot{\theta})\cos\theta - ml(-l\cos\theta\dot{\theta}^2 - l\sin\theta\ddot{\theta})\sin\theta = mgl\sin\theta - B_p(\dot{\theta}) \\ M\ddot{x} + m(\ddot{x} + l\sin\theta\dot{\theta}^2 - l\cos\theta\ddot{\theta}) = F - B_c(\dot{x}) \end{cases}$$

$$\begin{cases} ml^2\ddot{\theta} - ml\cos\theta\ddot{x} - mgl\sin\theta &= -B_p(\dot{\theta}) \\ (M+m)\ddot{x} + ml\sin\theta\dot{\theta}^2 - ml\cos\theta\ddot{\theta} &= F - B_c(\dot{x}) \end{cases} \quad , \qquad [\cdot] \tag{4.9}$$

which is the final dynamic equations for the cart pendulum system.

4.2 Energy Method

The energy method is applied to find the dynamic equations starting by using excessive coordinates. The potential and kinetic energy for the pendulum is,

$$U_p = mgh \qquad [\cdot] \tag{4.10}$$
$$T_p = \tfrac{1}{2}m\dot{x}_p^2 + \tfrac{1}{2}m\dot{y}_p^2 \quad , \qquad [\cdot] \tag{4.11}$$

Where:

U_p	is the potential energy of the pendulum	$[\cdot]$
T_p	is the kinetic energy of the pendulum	$[\cdot]$
h	is the height of the pendulum point mass	[m]

where the height, h, is given in relation to the pendulum at rest at $\theta = \pm\pi n$ by,

$$h = l(1 + \cos\theta) \quad . \qquad [\cdot] \tag{4.12}$$

The potential and kinetic energy in excessive coordinates for the cart is,

$$U_c = 0 \qquad [\cdot] \tag{4.13}$$
$$T_c = \tfrac{1}{2}M\dot{x}_c^2 \quad . \qquad [\cdot] \tag{4.14}$$

Where:

U_c	is the potential energy of the cart	$[\cdot]$

T_c is the kinetic energy of the cart $[\cdot]$

There is no potential energy for the cart as it is constrained at $y_c = 0$.
The combined energies for the system in excessive coordinates is then,

$$U = mgl(1 + \cos\theta) + 0 \quad [\cdot] \quad (4.15)$$
$$T = \tfrac{1}{2}m\dot{x}_p^2 + \tfrac{1}{2}m\dot{y}_p^2 + \tfrac{1}{2}M\dot{x}_c^2 \quad , \quad [\cdot] \quad (4.16)$$

Using the coordinate transformation from Equation 4.7 and 4.8 to obtain the energies of the system in generalized coordinates,

$$\begin{cases} U &= mgl(1 + \cos\theta) + 0 \\ T &= \tfrac{1}{2}m(\dot{x} - l\cos\theta\dot{\theta})^2 + \tfrac{1}{2}m(-l\sin\theta\dot{\theta})^2 + \tfrac{1}{2}M\dot{x}^2 \end{cases}$$

$$\begin{cases} U &= mgl(1 + \cos\theta) \\ T &= \tfrac{1}{2}(M+m)\dot{x}^2 - m\dot{x}l\cos\theta\dot{\theta} + \tfrac{1}{2}ml^2\dot{\theta}^2 \quad , \end{cases} \quad [\cdot] \quad (4.17)$$

By Equation 4.17 the Lagrangian becomes,

$$\mathcal{L} = T - U$$
$$\mathcal{L} = \tfrac{1}{2}(M+m)\dot{x}^2 - m\dot{x}l\cos\theta\dot{\theta} + \tfrac{1}{2}ml^2\dot{\theta}^2 - mgl(1 + \cos\theta) \quad . \quad [\mathrm{N}\cdot\mathrm{m}] \quad (4.18)$$

Where:

$\mathcal{L}$ is the Lagrangian $[\mathrm{N}\cdot\mathrm{m}]$

From the energy method[2] we find the dynamic equations by,

$$\frac{\partial\mathcal{L}}{\partial\mathbf{q}} - \frac{d}{dt}\frac{\partial\mathcal{L}}{\partial\dot{\mathbf{q}}} = 0 \quad . \quad (4.19)$$

Where:

$\mathbf{q}$ is the generalized coordinates, $[\ \theta \quad x\ ]^T$

$\dot{\mathbf{q}}$ is the generalized velocities, $[\ \dot{\theta} \quad \dot{x}\ ]^T$

In order to include external forces [3] d'Alambert principle,

$$\frac{d}{dt}\frac{\partial\mathcal{L}}{\partial\dot{\mathbf{q}}} - \frac{\partial\mathcal{L}}{\partial\mathbf{q}} = \mathbf{Q} \quad . \quad (4.20)$$

[2] FiXme Note: source and thermonology on energy method
[3] FiXme Note: add formal mumbojumbo

Where:

Q is the external forces, $[\ -B_p(\dot{\theta})\ \ F - B_c(\dot{x})\ ]^T$

For yields the final two dynamic equations, one for each of the generalized coordinates,

$$\begin{cases} \frac{d}{dt}\frac{\partial \mathcal{L}}{\partial \dot{\theta}} - \frac{\partial \mathcal{L}}{\partial \theta} & = m\dot{x}l\sin\theta\dot{\theta} - ml\cos\theta\ddot{x} + ml^2\ddot{\theta} - m\dot{x}l\sin\theta\dot{\theta} - mgl\sin\theta \\ \frac{d}{dt}\frac{\partial \mathcal{L}}{\partial \dot{x}} - \frac{\partial \mathcal{L}}{\partial x} & = (M+m)\ddot{x} + ml\sin\theta\dot{\theta}^2 - ml\cos\theta\ddot{\theta} - 0 \end{cases}$$

$$\begin{cases} ml^2\ddot{\theta} - ml\cos\theta\ddot{x} - mgl\sin\theta = -B_p(\dot{\theta}) \\ (M+m)\ddot{x} + ml\sin\theta\dot{\theta}^2 - ml\cos\theta\ddot{\theta} = F - B_c(\dot{x}) \quad , \end{cases} \qquad [\cdot] \quad (4.21)$$

which is the same result as achieved by Newton's method, as seen by comparing Equation 4.9 and 4.21.

4.3 Friction and Motor Model

In the previous, the friction is represented as functions of velocities, $B_c(\dot{x})$ and $B_p(\dot{\theta})$. The frictions are assumed to consist solely of Coulomb and viscous friction. This is a fairly simplified friction model and while it might be advantageous to include further friction dynamics, such as stiction and Stribeck friction, it is considered to be out of scope in this project. [4]

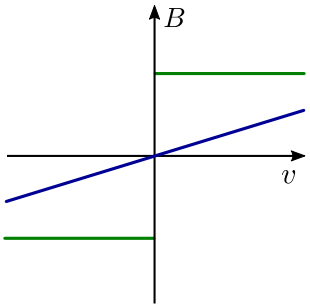

Figure 4.5:
coulombViscous1

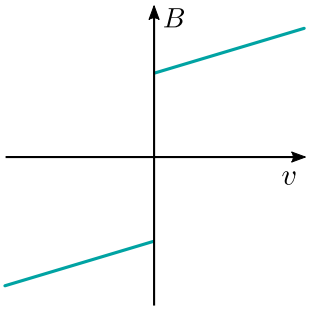

Figure 4.6:
coulombViscous2

The Coulomb and viscous friction as sketched in Figure 4.5 and 4.6 are described by the following relations for the pendulum and cart respectively,

$$B_p(\dot{\theta}) = b_{p,v}\dot{\theta} + \mathrm{sgn}(\dot{\theta})b_{p,c} \qquad [\mathrm{N}] \quad (4.22)$$

$$B_c(\dot{x}) = b_{c,v}\dot{x} + \mathrm{sgn}(\dot{x})b_{c,c} \quad . \qquad [\mathrm{N}] \quad (4.23)$$

Where:

$b_{p,v}$ is the pendulum viscous friction $[\mathrm{N}\cdot\mathrm{m}\cdot\mathrm{s}]$

[4] FiXme Note: friction sorurce

$b_{p,c}$	is the pendulum coulomb friction	$[\mathrm{N} \cdot \mathrm{m}]$
$b_{c,v}$	is the cart viscous friction	$[\mathrm{N} \cdot \mathrm{m}^{-1} \cdot \mathrm{s}]$
$b_{c,c}$	is the cart coulomb friction	$[\mathrm{N}]$

The sign-function used in Equation 4.23 is undesired, as it introduces a discontinuity at zero velocity. A commonly used continuous approximation of the Coulomb friction is achieved using a tanh-function with a constant, $\mathrm{k}_{\tanh}$, to adjust the curve's steepness around zero.

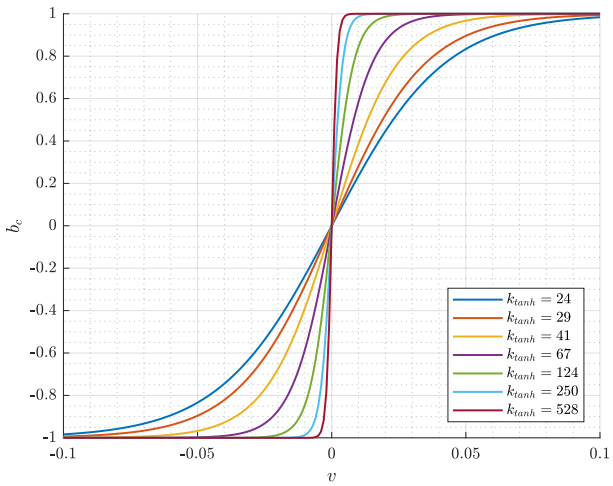

Figure 4.7: tanhApprox

Figure 4.7 shows the tanh approximation with different values of $\mathrm{k}_{\tanh}$. The friction parameters were estimated by a previous group who chose $\mathrm{k}_{\tanh} = 250$, so it makes sense to choose the same. Further, by comparing the curves in Figure 4.7 the choice of $\mathrm{k}_{\tanh}$ seems a reasonable compromise between size of constant and steepness of the curve. The final friction model is then given by,

$$B_p(\dot{\theta}) = b_{p,v}\dot{\theta} + \tanh(\mathrm{k}_{\tanh}\dot{\theta})b_{p,c} \quad [\mathrm{N}] \quad (4.24)$$

$$B_c(\dot{x}) = b_{c,v}\dot{x} + \tanh(\mathrm{k}_{\tanh}\dot{x})b_{c,c} \quad . \quad [\mathrm{N}] \quad (4.25)$$

The input force so far is represented by F, which is directly applied in the positive x direction on the cart. As seen in the beginning of this chapter in Figure 2.1, this force is applied by a motor mounted with a belt on pulleys. Because the motor control unit[5] is set up in current control mode the electrical motor dynamics are already accounted for. The controllable input is therefore the motor current, i_a. The torque, τ_m of the motor is modeled as directly proportional to the motor current by a torque constant, k_τ, as stated in *Motors* section 2.2,

$$\tau_m = k_\tau i_a \quad [\mathrm{N} \cdot \mathrm{m}] \quad (4.26)$$

[5] FiXme Note: refer system description

To translate this torque to the belt it is divided by the radius, r, of the pulley,

$$F = \frac{1}{r} k_\tau i_a \quad \text{[N]} \quad (4.27)$$

4.4 Parameters

As mentioned, some parameters could not be measured directly. These parameter were estimated by a previous group[6]. A table of the values they estimated along with directly measurable values are stated in Table 4.1.

Parameter		**Notation**	**Quantity**	**Unit**
Pendulum Mass		m		kg
Cart Mass	*	M		kg
Rod Length		l		m
Pulley Radius		r		m
Cart Coulomb Friction	*	$b_{c,c}$		N
Cart Viscous Friction	*	$b_{c,v}$		N·m^{-1}·s
Pendulum Coulomb Friction	*	$b_{p,c}$		N·m
Pendulum Viscous Friction	*	$b_{p,v}$		N·m·s

Table 4.1: '*' indicates that the parameter is estimated.

Though the inertia of the rotor is stated in the datasheet of the motor, see *Motors* section 2.2, the added inertia and mass of from the pulley and belt is unknown. Further, both viscous and Coulomb friction on the cart are assumed purely translational. Similarly, though the weights of motor and motor controller mounted on the cart are known, the collective weight of the cart is unknown. For these reasons, the cart weight, viscous and Coulomb friction were estimated by the previous group such that they include friction and inertia added by the motor, belt and pulleys.[7]

4.5 Simulation and Verification

A block diagram is derived in Figure 4.8 from

[6] FiXme Note: reference to their thesis
[7] FiXme Note: reference to old report

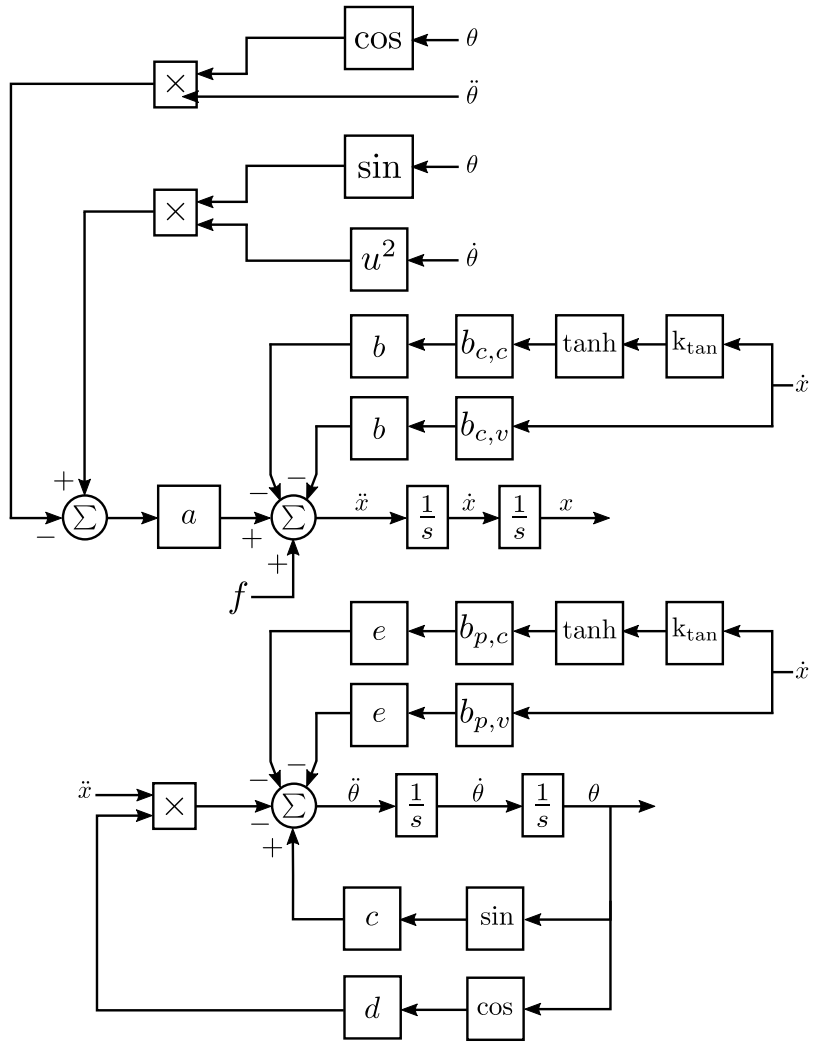

Figure 4.8: A block diagram derived from the dynamic equations, later used for simulation. Five signal connections, from $\dot{\theta}$, $\ddot{\theta}$, $\ddot{x}$ and two from θ, are drawn without explicit connection to keep the figure clear.

This is implemented in Matlab Simulink to simulate the system. A graphical layer, including the obstacles, is added to the simulation to show the system in action.

4.6 Nonlinear Analysis

In this section the nonlinear nature of the system is studied.[8]

It is possible to map trajectories in the $(\theta, \dot{\theta})$-plane assuming no applied force. To construct the phase portrait the dynamic equations, **??** and **??**, are combined. First $\ddot{x}$ is

[8] FiXme Note: name the tools used in the section

isolated in **??**,

$$\ddot{x} = -\frac{ml\cos\theta\ddot{\theta}}{M+m} + \frac{ml\sin\theta\dot{\theta}^2}{M+m} + \frac{f}{M+m} \quad . \tag{4.28}$$

This expression for $\ddot{x}$ is then substituted in **??** to obtain the dynamics in therms of the angle and its derivatives.

$$ml\cos\theta\left(-\frac{ml\cos\theta\ddot{\theta}}{M+m} + \frac{ml\sin\theta\dot{\theta}^2}{M+m} + \frac{f}{M+m}\right) + ml^2\ddot{\theta} - mlg\sin\theta = 0 \quad . \tag{4.29}$$

Rearranging yields,

$$\left(ml^2 - \frac{m^2l^2}{M+m}\cos^2\theta\right)\ddot{\theta} + \left(\frac{m^2l^2}{M+m}\sin\theta\cos\theta\right)\dot{\theta}^2 + f\frac{ml}{M+m}\cos\theta - mgl\sin\theta = 0 \quad , \tag{4.30}$$

which is the reduced system on the general form,

$$\alpha(\theta)\ddot{\theta} + \beta(\theta)\dot{\theta}^2 + \gamma(\theta) = 0 \quad , \tag{4.31}$$

where, $\alpha(\theta)$, $\beta(\theta)$ and $\gamma(\theta)$ are the scalar functions of θ from Equation 4.30.

Finally the reduced system on state space form, where $x_1 = \theta$ and $x_2 = \dot{\theta}$,

$$\begin{aligned} \dot{x_1} &= x_2 \\ \dot{x_2} &= -\frac{\beta(x_1)}{\alpha(x_1)}x_2^2 - \frac{\gamma(x_1)}{\alpha(x_1)} \quad . \end{aligned} \tag{4.32}$$

In Figure 4.9 the phase portrait is generated using pplane8.[9]

[9] FiXme Note: remove pplane8, redo plots

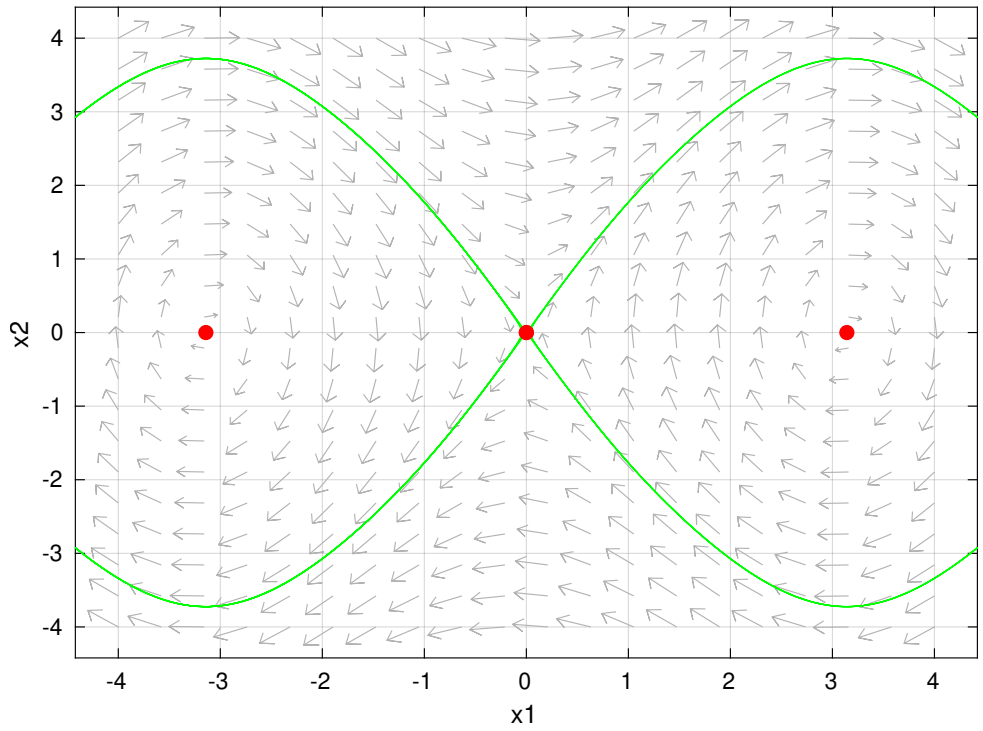

Figure 4.9: Phase portrait of the θ-dynamics, where $x_1 = \theta$ and $x_2 = \dot{\theta}$. The equilibrium points are shown in red and the unstable orbits at the saddle point are indicated in green.

As there is no friction in the system the pendulum will maintain one particular orbit around one of the center equilibrium points so long as the initial value is within the confines of the unstable orbit at the saddle point. This means that the pendulum will oscillate without loss of amplitude if the initial angular velocity, $\dot{\theta}$, is zero or at least places the starting point within the saddle.
If on the other hand the initial value of $\dot{\theta}$ is positive and θ is zero (upright position), then the pendulum will do full rotations around the cart, thus continuously increasing the angle.

If a force is imposed on the system it can change the phase portrait, allowing for other possible trajectories. This is further investigated in the following chapter.

5 | Nonlinear Control

The control objective is to stabilize the pendulum at $\theta = 0$. To achieve this objective a sliding mode controller is designed for the cart pendulum system. To do so the system is transformed into a *regular form* presented in this chapter along with the sliding mode design.

5.1 System Transformation

To develop a sliding mode controller, the system is first transformed into a *regular form*, [1]

$$\dot{\boldsymbol{\eta}} = f_a(\boldsymbol{\eta}, \boldsymbol{\xi}) \tag{5.1}$$

$$\dot{\boldsymbol{\xi}} = f_b(\boldsymbol{\eta}, \boldsymbol{\xi}) + g_b(\boldsymbol{\eta}, \boldsymbol{\xi})F \quad . \tag{5.2}$$

The system is first presented on nonlinear state space form, from Equation 4.21,

$$\begin{bmatrix} ml^2 & -ml\cos\theta \\ -ml\cos\theta & M+m \end{bmatrix} \begin{bmatrix} \ddot{\theta} \\ \ddot{x} \end{bmatrix} + \begin{bmatrix} -mgl\sin\theta \\ ml\sin\theta\dot{\theta}^2 \end{bmatrix} = \begin{bmatrix} -B_p(\dot{\theta}) \\ F - B_c(\dot{x}) \end{bmatrix} \tag{5.3}$$

By rearranging Equation 5.3,

$$\begin{bmatrix} ml^2 & -ml\cos\theta \\ -ml\cos\theta & M+m \end{bmatrix} \begin{bmatrix} \ddot{\theta} \\ \ddot{x} \end{bmatrix} + \begin{bmatrix} 0 \\ ml\sin\theta\dot{\theta}^2 \end{bmatrix} + \begin{bmatrix} B_p(\dot{\theta}) \\ B_c(\dot{x}) \end{bmatrix} + \begin{bmatrix} -mgl\sin\theta \\ 0 \end{bmatrix} = \begin{bmatrix} 0 \\ F \end{bmatrix} \quad , \tag{5.4}$$

the achieved form is that of the general dynamic equations for an m-link robot, [1, 2]

$$\mathbf{M}(\mathbf{q})\ddot{\mathbf{q}} + \mathbf{C}(\mathbf{q}, \dot{\mathbf{q}}) + \mathbf{B}(\dot{\mathbf{q}}) + \mathbf{G}(\mathbf{q}) = \mathbf{F} \quad . \tag{5.5}$$

Where:

$\mathbf{M}(\mathbf{q})\ddot{\mathbf{q}}$	is the inertia matrix
$\mathbf{C}(\mathbf{q}, \dot{\mathbf{q}})$	is the Coriolis and centrifugal effects
$\mathbf{B}(\dot{\mathbf{q}})$	is the friction
$\mathbf{G}(\mathbf{q})$	is the force due to gravity
$\mathbf{F}$	is the input force

Isolating the accelerations,

$$\ddot{\mathbf{q}} = \mathbf{M}^{-1}(\mathbf{q})\left(\mathbf{F} - \mathbf{C}(\mathbf{q}, \dot{\mathbf{q}}) - \mathbf{B}(\dot{\mathbf{q}}) - \mathbf{G}(\mathbf{q})\right) \quad , \tag{5.6}$$

[1] FiXme Note: source

and choosing the state vector to be $[\ x_1\ x_2\ x_3\ x_4\ ]^T = [\ \theta\ x\ \dot{\theta}\ \dot{x}\ ]^T$, the nonlinear state space representation is then,

$$\begin{bmatrix} \dot{x_1} \\ \dot{x_2} \\ \dot{x_3} \\ \dot{x_4} \end{bmatrix} = \begin{bmatrix} x_3 \\ x_4 \\ \mathbf{M}^{-1}(x_1)\left(-\mathbf{C}(x_1, x_3) - \mathbf{B}(x_3, x_4) - \mathbf{G}(x_1)\right) \end{bmatrix} + \begin{bmatrix} 0 \\ 0 \\ \mathbf{M}^{-1}(x_1) \begin{bmatrix} 0 \\ F \end{bmatrix} \end{bmatrix} \quad , \tag{5.7}$$

where,

$$\mathbf{M}^{-1} = \frac{1}{\det(\mathbf{M})}\text{adj}(\mathbf{M}) = \begin{bmatrix} \frac{(M+m)}{l^2 m(M+m-m\cos^2 x_1)} & \frac{\cos x_1}{l(M+m-m\cos^2 x_1)} \\ \frac{\cos x_1}{l(M+m-m\cos^2 x_1)} & \frac{1}{M+m-m\cos^2 x_1} \end{bmatrix} \quad . \tag{5.8}$$

Introducing following notation,

$$\begin{bmatrix} \dot{x_1} \\ \dot{x_2} \\ \dot{x_3} \\ \dot{x_4} \end{bmatrix} = \underbrace{\begin{bmatrix} x_3 \\ x_4 \\ f_1(\mathbf{x}) \\ f_2(\mathbf{x}) \end{bmatrix}}_{f(\mathbf{x})} + \underbrace{\begin{bmatrix} 0 \\ 0 \\ \frac{\cos x_1}{l(M+m-m\cos^2 x_1)} \\ \frac{1}{M+m-m\cos^2 x_1} \end{bmatrix}}_{g(\mathbf{x})} F \quad . \tag{5.9}$$

where,

$$f_1(\mathbf{x}) = \frac{(M+m)(-B_p(x_3) + mgl\sin x_1)}{l^2 m(M+m-m\cos^2 x_1)} - \frac{\cos x_1(ml\sin x_1 x_3^2 + B_c(x_4))}{l(M+m-m\cos^2 x_1)} \tag{5.10}$$

$$f_2(\mathbf{x}) = \frac{\cos x_1(-B_p(x_3) + mgl\sin x_1)}{l(M+m-m\cos^2 x_1)} - \frac{ml\sin x_1 x_3^2 + B_c(x_4)}{M+m-m\cos^2 x_1} \quad , \tag{5.11}$$

to reduce notation in the derivation of the transformation into *regular form*.

Choosing the pendulum angle as the output s.t. $y = h(\mathbf{x}) = x_1$, the relative degree is found by,

$$\dot{y} = \dot{x_1} = x_3 \tag{5.12}$$

$$\ddot{y} = \dot{x_3} = f_1(\mathbf{x}) + \frac{\cos x_1}{l(M+m-m\cos^2 x_1)} F \quad , \tag{5.13}$$

where the output is found in the second derivative of the output, resulting in relative

degree of two, $\rho = 2$, which gives rise to the following transform [2],

$$T(\mathbf{x}) = \begin{bmatrix} \boldsymbol{\phi}(\mathbf{x}) \\ \hdashline \boldsymbol{\psi}(\mathbf{x}) \end{bmatrix} = \begin{bmatrix} \phi_1(\mathbf{x}) \\ \phi_2(\mathbf{x}) \\ \hdashline h(\mathbf{x}) \\ L_f h(\mathbf{x}) \end{bmatrix} = \begin{bmatrix} \phi_1(\mathbf{x}) \\ \phi_2(\mathbf{x}) \\ \hdashline x_1 \\ x_3 \end{bmatrix} \quad , \tag{5.14}$$

where $L_f h(\mathbf{x})$ is the *Lie derivative* of $h(\mathbf{x})$ along $f(\mathbf{x})$. The functions $\phi_i(\mathbf{x})$ are chosen such that they satisfy,

$$\frac{\partial \phi_i}{\partial \mathbf{x}} g(\mathbf{x}) = 0 \ , \quad \text{for } 1 \leq i \leq 2 \quad , \tag{5.15}$$

which ensures that the input cancels in $\frac{d\boldsymbol{\phi}}{dt} = \frac{\partial \boldsymbol{\phi}}{\partial \mathbf{x}}[f(\mathbf{x}) + g(\mathbf{x})F]$,

Both $\phi_1(\mathbf{x}) = x_1$ and $\phi_1(\mathbf{x}) = x_2$ would satisfy Equation 5.15, however $\phi_1(\mathbf{x}) = x_1$ would result in a rank defisit in $T(\mathbf{x})$, so $\phi_1(\mathbf{x}) = x_2$ is chosen. For $\phi_2(\mathbf{x})$, it follows from Equation 5.15 that,

$$\frac{\partial \phi_2}{\partial x_3} \cdot \frac{\cos x_1}{l(M + m - m\cos^2 x_1)} + \frac{\partial \phi_2}{\partial x_4} \cdot \frac{1}{M + m - m\cos^2 x_1} = 0 \tag{5.16}$$

$$\frac{\partial \phi_2}{\partial x_3} \cdot \frac{\cos x_1}{l(M + m - m\cos^2 x_1)} + \frac{\partial \phi_2}{\partial x_4} \cdot \frac{l}{l(M + m - m\cos^2 x_1)} = 0 \quad . \tag{5.17}$$

It is attempted to cancel the two therms in Equation 5.17 by choosing,

$$\frac{\partial \phi_2}{\partial x_3} = l \quad , \qquad \frac{\partial \phi_2}{\partial x_4} = -\cos x_1 \tag{5.18}$$

$$\phi_2 = l \int dx_3 - \cos x_1 \int dx_4 \tag{5.19}$$

$$\phi_2 = l x_3 - \cos x_1 x_4 + \mathrm{C}_1 \quad , \tag{5.20}$$

where C_1 is an integration constant. It is also required that $\phi(0) = 0$, so $\mathrm{C}_1 = 0$, resulting in the final transformation,

$$T(\mathbf{x}) = \begin{bmatrix} x_2 \\ l x_3 - \cos x_1 x_4 \\ x_1 \\ x_3 \end{bmatrix} \quad . \tag{5.21}$$

[2] FiXme Note: source

Locating the input in the derivative of the transform,

$$\frac{d}{dt}T(\mathbf{x}) = \begin{bmatrix} \dot{x}_2 \\ l\dot{x}_3 + \sin x_1 x_4 \dot{x}_1 - \cos x_1 \dot{x}_4 \\ \dot{x}_1 \\ \dot{x}_3 \end{bmatrix} \quad . \tag{5.22}$$

Both $\dot{x}_3$ and $\dot{x}_3$ contains the input, so the second element, $\frac{\partial}{\partial \mathbf{x}} T_2(\mathbf{x})$, is further evaluated by substitution of the state derivatives from Equation 5.9,

$$\frac{d}{dt}T_2(\mathbf{x}) = l(f_1(\mathbf{x}) + \tfrac{\cos x_1}{l(M+m-m\cos^2 x_1)}F) + \sin x_1 x_4 x_3 - \cos x_1 (f_2(\mathbf{x}) + \tfrac{1}{M+m-m\cos^2 x_1}F) \tag{5.23}$$

$$\frac{d}{dt}T_2(\mathbf{x}) = \sin x_1 x_4 x_3 + l f_1(\mathbf{x}) - \cos x_1 f_2(\mathbf{x}) \quad , \tag{5.24}$$

showing that the input only appears on the fourth element in the derivative of the transformation. This leads to choosing $[\ \phi_1\ \phi_2\ \psi_1\ \psi_2\ ]^T = [\ \eta_1\ \eta_2\ \eta_3\ \xi\ ]^T$, according to Equation 5.1 and 5.2, as the new variables, with its derivatives,

$$\begin{bmatrix} \dot{\eta}_1 \\ \dot{\eta}_2 \\ \dot{\eta}_3 \\ \hdashline \dot{\xi} \end{bmatrix} = \underbrace{\overbrace{\begin{bmatrix} x_4 \\ \sin x_1 x_4 x_3 + l f_1(\mathbf{x}) - \cos x_1 f_2(\mathbf{x}) \\ x_3 \\ \hdashline f_1(\mathbf{x}) \end{bmatrix}}^{f_a}}_{f_b} + \underbrace{\begin{bmatrix} 0 \\ 0 \\ 0 \\ \hdashline \frac{\cos x_1}{l(M+m-m\cos^2 x_1)} \end{bmatrix}}_{g_b} F \quad , \tag{5.25}$$

which is the system on *regular form*, however, to achieve the full change of variables, s.t.

$$\dot{\boldsymbol{\eta}} = f_a(\boldsymbol{\eta}, \xi) \tag{5.26}$$

$$\dot{\xi} = f_b(\boldsymbol{\eta}, \xi) + g_b(\boldsymbol{\eta}, \xi) F \quad , \tag{5.27}$$

the inverse transform is found,

$$\begin{bmatrix} \eta_1 \\ \eta_2 \\ \eta_3 \\ \xi \end{bmatrix} = \begin{bmatrix} x_2 \\ l x_3 - \cos x_1 x_4 \\ x_1 \\ x_3 \end{bmatrix} \qquad \begin{bmatrix} x_1 \\ x_2 \\ x_3 \\ x_4 \end{bmatrix} = \begin{bmatrix} \eta_3 \\ \eta_1 \\ \xi \\ \frac{l\xi - \eta_2}{\cos \eta_3} \end{bmatrix} \quad , \tag{5.28}$$

to then formulate Equation 5.25 in therms of $[\ \eta_1\ \eta_2\ \eta_3\ \xi\ ]^T$, [3]

$$\begin{bmatrix}\dot{\eta}_1\\ \dot{\eta}_2\\ \dot{\eta}_3\\ \dot{\xi}\end{bmatrix} = \begin{bmatrix}\frac{l\xi-\eta_2}{\cos\eta_3}\\ \frac{\sin\eta_3}{\cos\eta_3}(l\xi-\eta_2)\xi + lf_1(\boldsymbol{\eta},\xi) - \cos\eta_3 f_2(\boldsymbol{\eta},\xi)\\ \xi\\ f_1(\boldsymbol{\eta},\xi)\end{bmatrix} + \begin{bmatrix}0\\0\\0\\ \frac{\cos\eta_3}{l(M+m-m\cos^2\eta_3)}\end{bmatrix} F \quad , \tag{5.29}$$

where,

$$f_1(\boldsymbol{\eta},\xi) = \frac{(M+m)(mgl\sin\eta_3 - b_{p,v}\xi - \tanh(\mathrm{k}_{\tanh}\xi)b_{p,c})}{l^2 m(M+m-m\cos^2\eta_3)} \tag{5.30}$$

$$- \frac{\cos\eta_3(ml\sin\eta_3\xi^2 + b_{c,v}\frac{l\xi-\eta_2}{\cos\eta_3} + \tanh(\mathrm{k}_{\tanh}\frac{l\xi-\eta_2}{\cos\eta_3})b_{c,c})}{l(M+m-m\cos^2\eta_3)} \tag{5.31}$$

$$f_2(\boldsymbol{\eta},\xi) = \frac{\cos\eta_3(mgl\sin\eta_3 - b_{p,v}\xi - \tanh(\mathrm{k}_{\tanh}\xi)b_{p,c})}{l(M+m-m\cos^2\eta_3)} \tag{5.32}$$

$$- \frac{ml\sin\eta_3\xi^2 + b_{c,v}\frac{l\xi-\eta_2}{\cos\eta_3} + \tanh(\mathrm{k}_{\tanh}\frac{l\xi-\eta_2}{\cos\eta_3})b_{c,c}}{M+m-m\cos^2\eta_3} \quad . \tag{5.33}$$

5.2 Sliding Mode

Now, with the system on *regular form*, the sliding mode controller can be designed. The sliding manifold is chosen:

$$s = \xi - \phi(\boldsymbol{\eta}) = 0 \quad , \tag{5.34}$$

where $\phi(\boldsymbol{\eta})$ must be designed. When the system is restricted to move along $s = 0$ then $\xi = \phi(\boldsymbol{\eta})$, which means the reduced-order model,

$$\dot{\boldsymbol{\eta}} = f_a(\boldsymbol{\eta}, \phi(\boldsymbol{\eta})) \quad , \tag{5.35}$$

is asymptotically stable in its origin. To find a stabilizing controller, $\phi(\boldsymbol{\eta})$, for Equation 5.35, the reduced-order system is linearized,

$$A = \frac{\partial\dot{\boldsymbol{\eta}}}{\partial\boldsymbol{\eta}}\bigg|_{\substack{\boldsymbol{\eta}=\mathbf{0}\\ \xi=0\\ \mathrm{k}_{\tanh}=1}} = \begin{bmatrix}0 & -1 & 0\\ 0 & \frac{g_{p,c}}{lm} & g\\ 0 & 0 & 0\end{bmatrix} \quad , \quad B = \frac{\partial\dot{\boldsymbol{\eta}}}{\partial\xi}\bigg|_{\substack{\boldsymbol{\eta}=\mathbf{0}\\ \xi=0\\ \mathrm{k}_{\tanh}=1}} = \begin{bmatrix}l\\ \frac{-b_{p,v}-b_{p,c}}{lm}\\ 1\end{bmatrix} \quad , \tag{5.36}$$

Using the matlab *place()* command, different pole-placements were attempted, seen in Figure 5.1. The chosen pole placement is $[\ -3\quad -5\quad -8\ ]$ resulting in the state feedback gains, $\mathbf{k} = [\ -12.22\quad 8.05\quad 20.10\ ]$, of which the result is seen in Figure 5.2, where the linear simulation is achieved using *lsim()* and the nonlinear using *ode45*. [4]

[3] FiXme Note: word on diffeomorphism, inverse transform exist.. smthng.
[4] FiXme Note: fix formatting on matlab function reff.'s

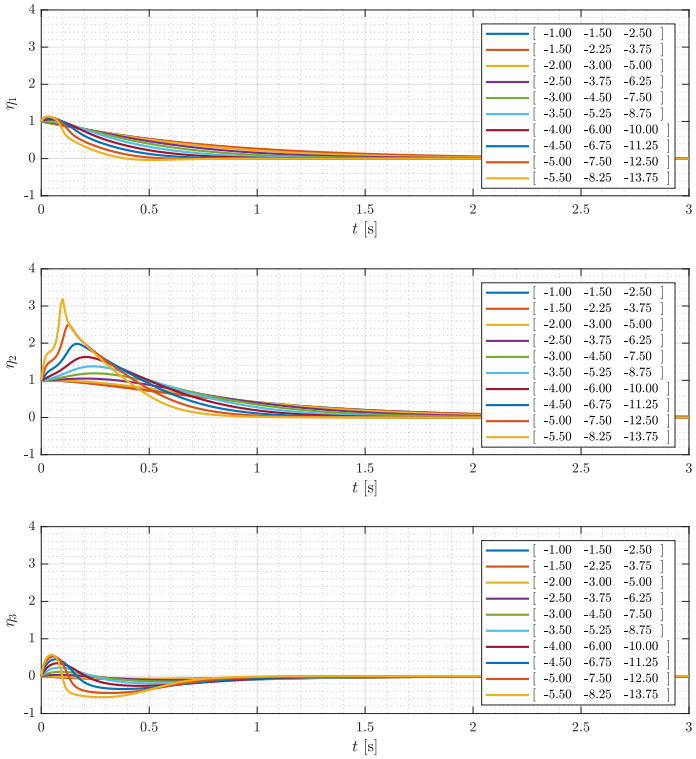

Figure 5.1: reducedOrderControlMany

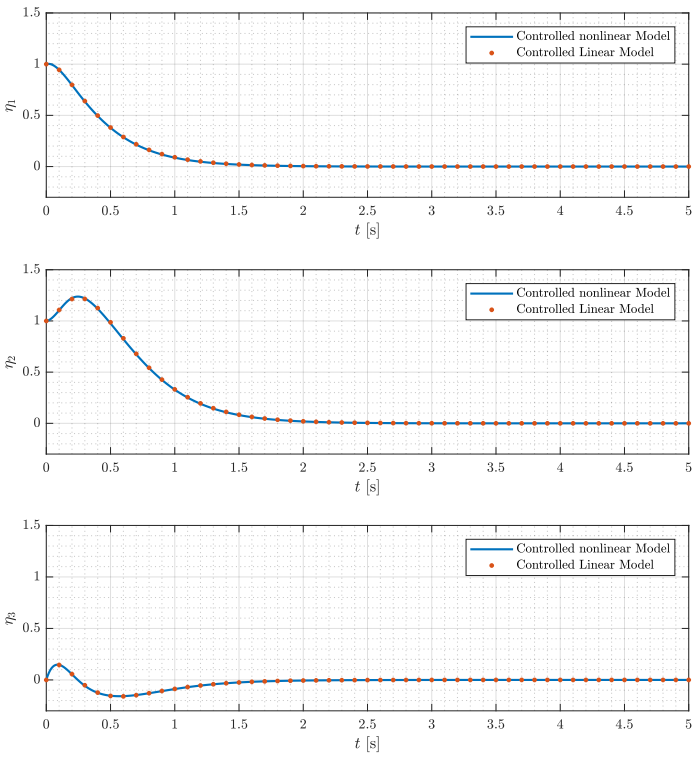

Figure 5.2: reducedOrderControl

With the reduced-order system stabilized by,

$$\phi(\boldsymbol{\eta}) = -\mathbf{k}\boldsymbol{\eta} \quad , \tag{5.37}$$

next step is to design F to bring s to zero.
First a Lyapunov function candidate, $V = \frac{1}{2}s^2$, is chosen and its derivative along the system's trajectories is found,

$$\dot{V} = s\dot{s} \tag{5.38}$$

$$\dot{V} = s(\dot{\xi} + \mathbf{k}\dot{\boldsymbol{\eta}}) \tag{5.39}$$

$$\dot{V} = s(f_b(\boldsymbol{\eta},\xi) + g_b(\boldsymbol{\eta},\xi)F + \mathbf{k}f_a(\boldsymbol{\eta},\xi)) \tag{5.40}$$

$$\dot{V} = (\mathbf{k}f_a(\boldsymbol{\eta},\xi) + f_b(\boldsymbol{\eta},\xi))s + g_b(\boldsymbol{\eta},\xi)sF \tag{5.41}$$

$$\dot{V} = g_b(\boldsymbol{\eta},\xi)s(\mathbf{k}f_a(\boldsymbol{\eta},\xi) + f_b(\boldsymbol{\eta},\xi))g_b^{-1}(\boldsymbol{\eta},\xi) + g_b(\boldsymbol{\eta},\xi)sF \tag{5.42}$$

$$\dot{V} \leq g_b(\boldsymbol{\eta},\xi)|s|\left|\mathbf{k}f_a(\boldsymbol{\eta},\xi)g_b^{-1}(\boldsymbol{\eta},\xi) + f_b(\boldsymbol{\eta},\xi)\right| + g_b(\boldsymbol{\eta},\xi)sF \quad . \tag{5.43}$$

Using that $|s| = \text{sgn}(s)s$ to design F such that the two terms in Equation 5.43 cancels and the stability criterion is fulfilled,

$$\begin{aligned}\dot{V} \leq\ & g_b(\boldsymbol{\eta},\xi)|s|\,|\mathbf{k}f_a(\boldsymbol{\eta},\xi) + f_b(\boldsymbol{\eta},\xi)|\,g_b^{-1}(\boldsymbol{\eta},\xi) \\ & - g_b(\boldsymbol{\eta},\xi)\text{sgn}(s)s\,|\mathbf{k}f_a(\boldsymbol{\eta},\xi) + f_b(\boldsymbol{\eta},\xi)|\,g_b^{-1}(\boldsymbol{\eta},\xi)\end{aligned} \tag{5.44}$$

s.t.

$$F = -\text{sgn}(s)\varrho(\boldsymbol{\eta},\xi)g_b^{-1}(\boldsymbol{\eta},\xi) \quad \text{where,} \quad \varrho(\boldsymbol{\eta},\xi) \geq |\mathbf{k}f_a(\boldsymbol{\eta},\xi) + f_b(\boldsymbol{\eta},\xi)| \quad , \tag{5.45}$$

further, a tuning parameter, β_0, is introduced,

$$F = -\text{sgn}(s)\beta(\boldsymbol{\eta}, \xi) \quad \text{where,} \quad \beta(\boldsymbol{\eta}, \xi) = \varrho(\boldsymbol{\eta}, \xi) + \beta_0 \quad . \tag{5.46}$$

The gain design is based on a maximum possible catch angle, $\theta_{\max}$, which is defined from zero angular velocity. The position and velocity along x does not interfere with the value of $\theta_{\max}$, so long as the angular velocity of the pendulum is zero. Note, if the pendulum is falling away from equilibrium, its non-zero angular velocity will work against the controller and the catch angle will be smaller. However, similarly, if the pendulum is approaching equilibrium, the controller's catch angle will be larger.
While there will be other combinations of θ and $\dot{\theta}$ in the region of interest requiring as much actuation as $(\theta, \dot{\theta}) = (\theta_{\max}, 0)$, these initial values are chosen to be on the edge of the region in the proceeding design.
In Figure 5.3, $\varrho(\boldsymbol{\eta}, \xi)$ and the required peak armature current magnitude, $|i_{a,\text{peak}}|$, are plotted for different initial angles, θinit, to see how large a gain is feasible while staying within the actuation limitation of the motor, $i_{a,\max} = 4.58\,\text{A}$, see *Motors* section 2.2.

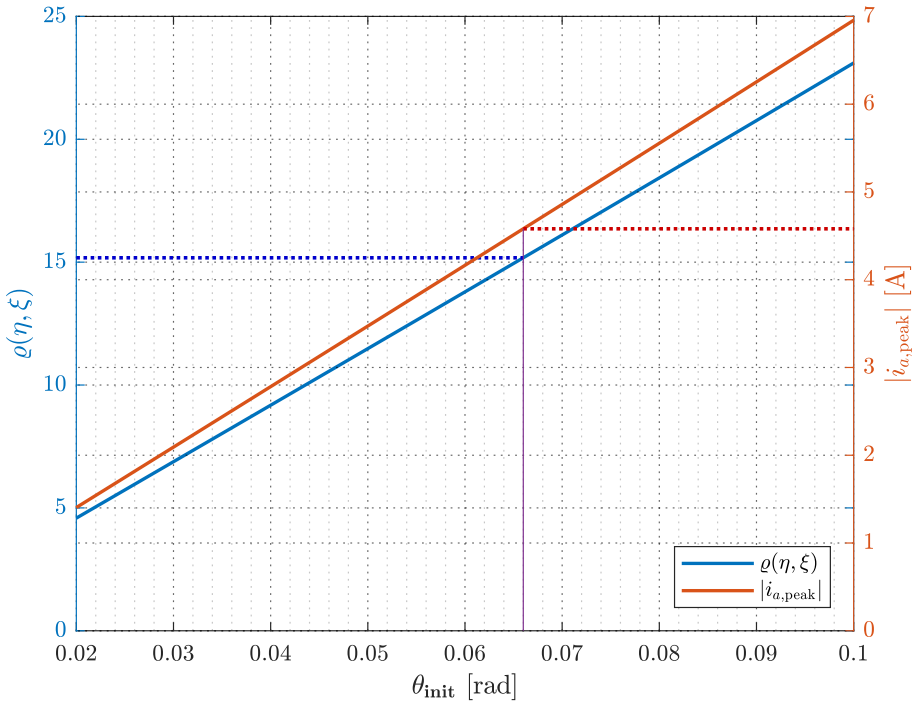

Figure 5.3: $\dot{\theta} = 0$ horizontal line marks $\theta_{\max} = 0.0660$ dictated by the current limitation of the motor, $i_{a,\max} = 4.58\,\text{A}$, and thereby indicating the maximum gain, $\varrho(\boldsymbol{\eta}, \xi) = 15.1776$, with $\beta_0 = 0.1$, allowing some margin for the supposed operational region.

6 | Trajectory Planning

In this chapter, the problem posed in **??**, Figure 3.1, is broken down into successive tasks. Each of these tasks are then analyzed to find feasible trajectories. These trajectories are finally realized and concatenated to finally accomplish the posed problem of obstacle avoidance.

6.1 Successive Trajectories

The first step in accomplishing the task would be to raise the pendulum high enough that it would be able to pass through the obstacles. It would be possible to clear a straight path through the obstacles by raising the pendulum from the starting position of $\theta = \pi$ to a little less than $\theta = \frac{\pi}{2}$. Further, the velocity would ideally achieve zero angular velocity as it reaches its target angle. This idea is presented in Figure 6.1, without restricting the pendulum to a specific trajectory but rather showing the initial and final conditions.

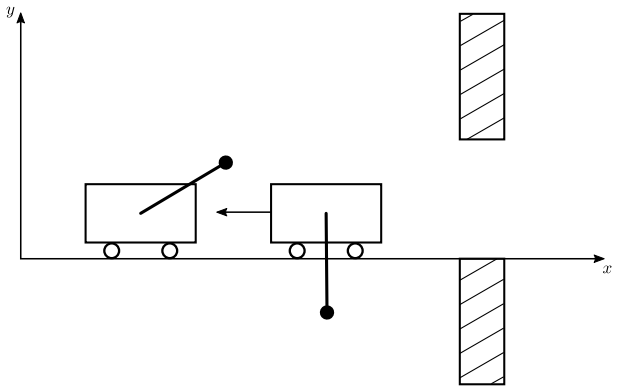

Figure 6.1: The first task is to find a trajectory which raises the pendulum to a position where it is clear of the obstacles in the horizontal direction. Further, to maintain clearance, the angular velocity should hit zero as the target angle is achieved.

The phase portrait in Figure 4.9, showing the natural theta-dynamics, it is possible to get an idea of how the pendulum moves. The starting position would be the right-most equilibrium of the phase portrait. If this task should be achieved without external force, the pendulum would have to be initialized in the orbit containing the desired final values. However, by exerting a force on the cart it is possible to shift the theta-dynamics. This is further investigated in the following section.

Assuming that the pendulum was raised above $\frac{\pi}{2}$ while briefly achieving zero angular velocity, the next task would be to maintain zero angular velocity while moving the cart, passing the pendulum through the obstacles, see Figure 6.2.

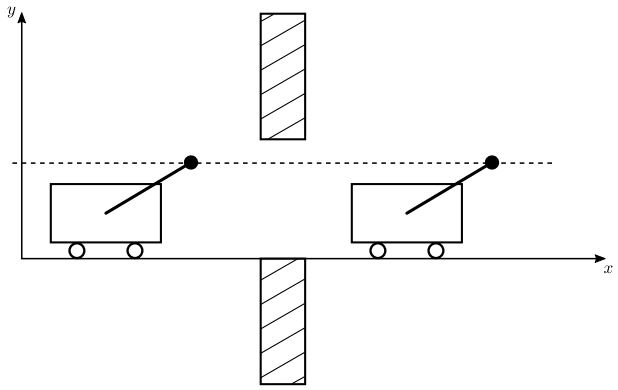

Figure 6.2: The second task is to find a trajectory which keeps the angle and angular velocity at zero as the pendulum is moved with the cart through the obstacles. This can be seen as a virtual constraint where the pendulum is mass is constrained to the dotted line.

Ideally this trajectory is a straight horizontal line. This can be seen as a virtual constraint that forces the angle and the angular velocity to stay unchanged. The result will be significantly reduced dynamics, which can be used to directly achieve the desired trajectory.

Finally it is necessary to recover the system on the other side of the obstacles. It is found that this can be achieved, to some extend, by reversing the first trajectory.

6.2 First Trajectory

Firstly the initial and final values of of θ and $\dot{\theta}$ are known. Further, the θ-dynamics are known, also for non-zero forces. In the state space and general equations, Equation 4.32 and Equation 4.31, the input force is contained by the γ-function.
If now Equation 4.31 is seen as an initial value problem. After some manipulation, [1] [2] it is seen that the following function preserves its zero value along the trajectory from initial to final value, assuming the solution exists while requiring α to be non-zero,

$$\dot{\theta}^2 - \psi(\theta_0, \theta)\left(\dot{\theta}_0^2 - \int_{\theta_0}^{\theta} \psi(\theta_0, \theta)\frac{2\gamma(s)}{\alpha(s)}ds\right) = 0 \quad , \tag{6.1}$$

where,

$$\psi(\theta_0, \theta) = \exp\left\{-2\int_{\theta_0}^{\theta}\frac{\beta(\tau)}{\alpha(\tau)}d\tau\right\} \quad .$$

It turns out, that in this case the problem can be solved analytically, and by requiring

[1] FiXme Note: source Anton's paper(s)
[2] FiXme Note: maybe include further explanation/derivations

the final value of the angular velocity be zero, it boils down to,

$$\left[-f\frac{ml}{M+m}\sin(s) - mgl\cos(s)\right]_{\theta_0}^{\theta} = 0 \quad . \tag{6.2}$$

Inserting initial and final value of θ and solving for f, the force which creates the desired trajectory is obtained. Also note that for this trajectory the applied force is constant and negative, pulling the cart to the left.

Going back to the θ-dynamics, it is possible to construct a phase portrait, see Figure 6.3, including this negative constant force.

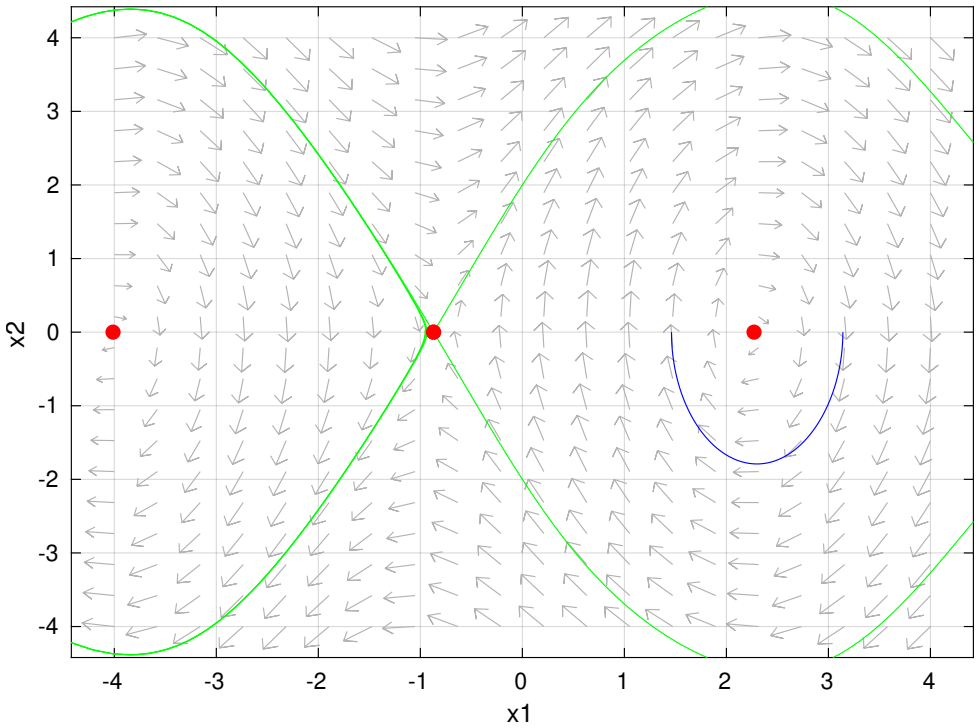

Figure 6.3: Phase portrait of the θ-dynamics including a constant applied force, where $x_1 = \theta$ and $x_2 = \dot{\theta}$. The phase portrait is shifted negatively along θ because of the applied force. This allows the desired trajectory (blue) from the initial downward position.

Note how the entire phase portrait is shifted in the negative θ (x_1) direction. This could be expected from Equation 4.30, since the force only scales the magnitude of a term which otherwise only depends on θ. Further, the constant force applied is negative, thus the negative shift in the θ direction.
This shift of the phase portrait means that the initial downward position of the pendulum now is placed in an orbit rather than an equilibrium.
Additionally, the trajectory (blue) reaches zero angular velocity just as it hits the target angle. The trajectory does however not stop there. It oscillates around the new center equilibrium. Therefore the next input force for the next trajectory must be applied the moment zero angular velocity is achieved.

6.3 Second Trajectory

The second trajectory to complete the task seen in Figure 6.2 is different that the first, in that it does not require movement in the $(\theta, \dot{\theta})$-plane, in fact, rather the contrary. It does however require the cart to move forward in order to pass the obstacles and hold up the pendulum.
As before, the initial values are known and a final position of the cart can be chosen, which will be the condition for switching to the final task.
Substituting the initial values, $\theta = \theta_t$ (target angle), $\dot{\theta} = 0$ and $\ddot{\theta} = 0$, into the dynamic equations, **??** and **??**, reduces to,

$$ml \cos\theta_t \, \ddot{x} - mlg \sin\theta_t = 0 \tag{6.3}$$

$$(M + m)\ddot{x} = f \quad . \tag{6.4}$$

In Equation 6.4 the force, f, is directly provided as a function of the acceleration of the cart. Feeding back $\ddot{x}$ in this manner will attempt to keep the angle of the pendulum steady while moving forward through the obstacles.
It is interesting to note that the average of the force excreted during this second trajectory changes the θ-dynamics in such a way that the angle and angular velocity are kept in a saddle point equilibrium.

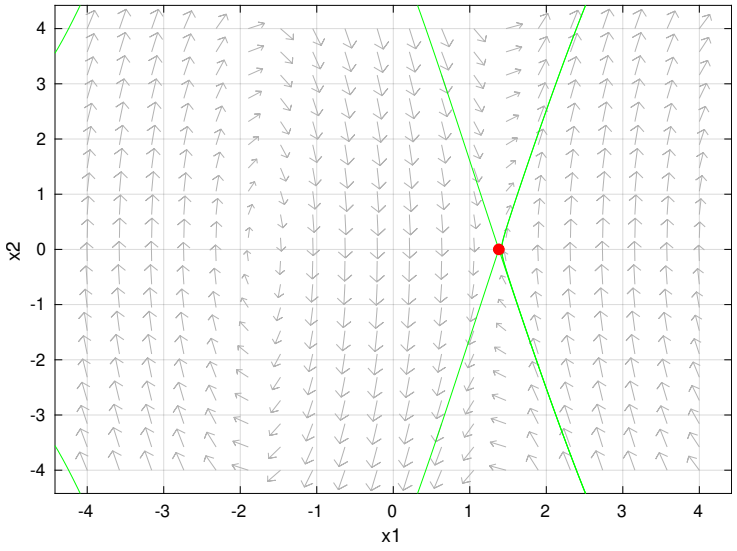

Figure 6.4: Phase portrait showing how the θ-dynamics changes given a constant force averaged from the forces used during the second trajectory. The system is kept near the indicated saddle point equilibrium.

6.4 Third Trajectory

Bibliography

[1] Mark W. Spong, Seth Hutchinson, and M. Vidyasagar. *Robot Dynamics and Control*. 2nd ed. Wiley, 2005.

[2] Lorenzo Sciavicco and Bruno Siciliano. *Modelling and Control of Robot Manipulators*. 2nd ed. Lorenzo Sciavicco and Bruno Siciliano. London: Springer, 2012.

List of Corrections